ACS APPLIED MATERIALS & INTERFACES

Research Article

www.acsami.org

# Carrier Lifetime Extension via the Incorporation of Robust Hole/Electron Blocking Layers in Bulk Heterojunction Polymer Solar Cells

Youngwoon Yoon,[†] Hyeong Jun Kim,[‡] Chul-Hee Cho,[‡] Seulki Kim,[§] Hae Jung Son,[†] Min-Jae Ko,[†] Honggon Kim,[†] Doh-Kwon Lee,[†] Jin Young Kim,[†] Wonmok Lee,[§] Bumjoon J. Kim,[‡] and BongSoo Kim*,[†]

[†]Photo-electronic Hybrids Research Center, Korea Institute of Science and Technology, Seoul 136-791, Republic of Korea

[‡]Department of Chemical and Biomolecular Engineering, Korea Advanced Institute of Science and Technology (KAIST), Daejeon 305-701, Republic of Korea

[§]Department of Chemistry, Sejong University, Gunja-dong, Gwangjin-gu, Seoul 143-747, Republic of Korea

Supporting Information

**ABSTRACT:** We report the achievement of a power conversion efficiency (PCE) improvement in P3HT:PCBM-based bulk-heterojunction type polymer solar cells using photocrosslinked P3HT (c-P3HT) as the electron blocking/hole extraction layer and titanium oxide nanoparticles ($TiO_2$) as the hole blocking/electron extraction layer. Devices prepared with a 20 nm thick c-P3HT layer showed an improved PCE of 3.4% compared to devices prepared without the c-P3HT layer (PCE = 3.0%). This improvement was attributed to an extension in the carrier lifetime and an enhancement in the carrier mobility. The incorporation of the c-P3HT layer lengthened (by more than a factor of 2) the carrier lifetime and increased (by a factor of 5) the hole mobility. These results suggest that the c-P3HT layer not only prevented non-geminate recombination but it also improved carrier transport. The PCE was further improved to 4.0% through the insertion of a $TiO_2$ layer that acted as an effective hole-blocking layer at the interface between the photoactive layer and the cathode. This work demonstrates that the incorporation of solution-processable hole and electron blocking/extraction layers offers an effective means for preventing nongeminate recombination at the interfaces between a photoactive layer and an electrode in bulk-heterojunction-type polymer solar cells.

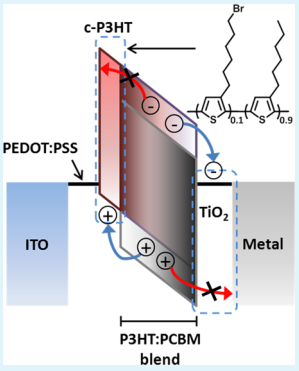


**KEYWORDS:** *organic photovoltaics, polymer solar cells, power conversion efficiency, hole mobility, carrier lifetime, recombination rate*

## INTRODUCTION

Organic photovoltaic cells (OPVs) have been intensively studied due to their unique advantageous properties relating to their low weight, good flexibility, and low-cost production via roll-to-roll processes.[1−6] Recent developments in OPV materials and device fabrication techniques have increased the power conversion efficiencies (PCEs) of such devices beyond 7%.[7−12] Bulk heterojunction (BHJ)-type photoactive layers have been widely employed to overcome the short exciton diffusion length (~10 nm), typical of organic materials.[13,14] In an ideal BHJ-type photoactive layer, electron donors and electron acceptors form nanoscale interpenetrating networks that generate a large interfacial area between the electron donor/electron acceptor materials while maintaining good carrier transport properties. One of the most widely studied BHJ OPV systems is based on a blend of poly(3-hexylthiophene) (P3HT) as the electron donor and [6,6]-phenyl-C61-butyric acid methyl ester (PCBM) as the electron acceptor.[15−17] Several fabrication processes, including post thermal annealing and solvent annealing, have been applied to the development of the nanoscale phase-separated morphology in the P3HT:PCBM BHJ layer. The P3HT:PCBM devices typically suffer from the formation of an undesirable vertical distribution of materials between the two electrodes. The differences between the surface energies of P3HT (25.8 mN/m) and PCBM (39.9 mN/m) tend to favor the formation of a P3HT-rich region at the top (air) surface, whereas a PCBM-rich region remains on the bottom (substrate) surface.[18−21] The hydrophilic poly(3,4-ethylenedioxythiophene):poly(styrenesulfonate) (PEDOT:PSS) layer (68.5 mN/m) interacts more favorably with PCBM molecules.[22] The unfavorable vertical phase separation induces nongeminate recombination, especially at the interfaces between the P3HT:PCBM blend and the electrodes, significantly reducing the short-circuit current, fill factor, and open-circuit voltage.[23,24]

To address the issues associated with the undesirable component distribution, electron or hole-blocking layers have been introduced.[25−30] For instance, thermally evaporated $C_{60}$,[25] a crosslinkable $C_{60}$ derivative,[31] and metal oxides (e.g., $TiO_2$ and ZnO)[32−35] have been used as hole-blocking/electron extraction layers. Small molecules,[33] polymers,[22] grapheme oxides,[36] and metallic nanoparticles[37] have also been used as

Received: October 6, 2013
Accepted: November 20, 2013
Published: November 20, 2013

  

electron blocking/hole extraction layers. In particular, Oh et al. demonstrated that a P3HT layer inserted using transfer printing techniques produced a favorable vertical phase separation in a P3HT:PCBM blend film because it changed the surface properties from hydrophilic to hydrophobic;[22] however, this approach required multistep processes and was not applicable to large-area device fabrication. Therefore, it is important to develop a facile means for forming a robust thin electron blocking/hole extraction layer between a PEDOT:PSS layer and a photoactive layer.

In this report, we introduced a photocrosslinked P3HT (c-P3HT) interlayer between the PEDOT:PSS and the photoactive layer to form a device having the following structure: ITO/PEDOT:PSS/c-P3HT/P3HT:PCBM/Al. We investigated the device performance as a function of the c-P3HT layer thickness. The PCE values of the device prepared with a 20 nm thick c-P3HT layer were improved from 3.0% to 3.4%. Space–charge limited current (SCLC) measurements, transient photovoltage (TPV) measurements, and impedance spectroscopy measurements revealed that the inserted c-P3HT interlayer effectively increased the charge-carrier mobility and charge carrier lifetime, thus suppressing non-geminate recombination. Finally, with the addition of a hole blocking/electron extraction $TiO_2$ layer, the device was optimized to give a PCE value of 4.0%. This work demonstrates that the combinatorial use of a robust c-P3HT and a $TiO_2$ layer offers an effective means for improving the solar cell performance.

## EXPERIMENTAL SECTION

**Photovoltaic Device Fabrication.** ITO glass substrates were cleaned by sonication in isopropanol, acetone, and isopropanol for 10 min each and dried under a stream of nitrogen. The ITO glass substrates were treated with UV/ozone for 20 min before spin-coating poly(3,4-ethylenedioxythiophene):poly(styrenesulfonate) (PEDOT:PSS) solution. The PEDOT:PSS solution was purchased from Clevios (AI4083, Germany) and diluted with methanol by 1:1 volume ratio prior to use. The resulting solution produced a 30 nm-thick PEDOT:PSS layer by spin-coating at a speed of 4000 rpm for 35 s. The PEDOT:PSS-coated ITO glass substrates were dried in a vacuum oven at 120 °C for 10 min. The photocrosslinkable P3HT (P3HT-Br10, see the structure in Figure 1a) was synthesized as reported previously.[38,39] A P3HT-Br10 solution in chlorobenzene was then spin-coated onto the ITO/PEDOT:PSS substrate. The thickness of the c-P3HT interlayer varied from 15 to 40 nm by controlling the P3HT-Br10 solution concentration and the spin-coating speed. The P3HT-Br10 polymer films were crosslinked under an UV lamp (254 nm, 30 mW/cm$^2$) for 1 min under nitrogen atmosphere. For the P3HT:PCBM BHJ active layer, the P3HT:PCBM blend solution (1:0.6 wt/wt) was prepared with a polymer:PCBM blend concentration of ~19.2 mg/mL and was stirred at RT overnight. The P3HT:PCBM blend solution was spin-coated on top of the c-P3HT interlayer at a speed of 800 rpm for 15 s. For the formation of $TiO_2$ nanoparticle layer as a hole blocking/electron extraction layer, 5 nm-sized $TiO_2$ nanoparticles were dispersed in ethanol at a concentration of 0.4 wt % and spin-coated on top of the P3HT:PCBM layer at a speed of 4000 rpm for 25 s.[40] Lastly, a 100 nm thick Al cathode was deposited by thermal evaporation under vacuum ($10^{-6}$ Torr). Post-thermal annealing was then performed in the thermal evaporator at 150 °C for 10 min without breaking the vacuum condition.

**Characterizations.** Current density versus voltage ($J$–$V$) characteristics were recorded on a Keithley model 2400 source measuring unit. A class A solar simulator with a 150 W xenon lamp (Newport) equipped with a KG-5 filter served as a light source. Its light intensity was adjusted to AM 1.5 G 1 sun light intensity using a NREL-calibrated mono Si solar cell. External quantum efficiency (EQE) was measured as a function of wavelength from 300 to 800 nm on incident photon-to-current conversion equipment (PV measurement Inc.). Calibration was performed using a silicon photodiode G425, which is NIST-calibrated as a standard. The surface of ITO/PEDOT:PSS layer, c-P3HT interlayer, and P3HT:PCBM layer were imaged using an atomic force microscopy (AFM, XE-100, Park Systems) in the tapping mode.

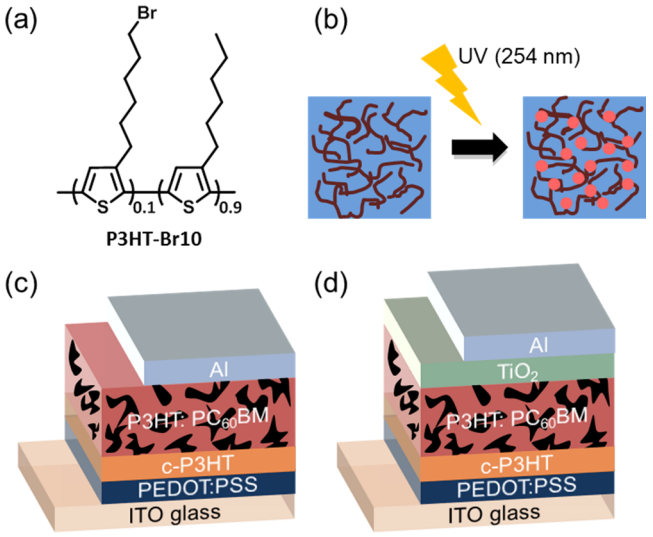


**Figure 1.** (a) Chemical structure of photocrosslinkable P3HT (P3HT-Br10), (b) schematic representation of the photocrosslinking process, (c) device structure of ITO/PEDOT:PSS/c-P3HT/P3HT:PCBM/Al, and (d) device structure of ITO/PEDOT:PSS/c-P3HT/P3HT:PCBM/$TiO_2$ nanoparticle/Al.

For hole mobility measurements, hole only devices were fabricated with a structure of ITO/PEDOT:PSS/P3HT:PCBM blend film/Au or ITO/PEDOT:PSS/c-P3HT/P3HT:PCBM blend film/Au. Hole mobilities were determined from $J$–$V$ curves in the dark by the space charge limited current (SCLC) method, based on the following equation:

$$J = \frac{9}{8}\varepsilon_r\varepsilon_0\mu_h\frac{V^2}{L^3} \quad (1)$$

where $\varepsilon_0$ is the permittivity of free space, $\varepsilon_r$ is the dielectric constant of the P3HT:PCBM blend film (3.5, extracted from impedance measurement in dark), $\mu_h$ is the hole mobility, $V = V_{appl} - V_{bi} - V_a$ ($V_{appl}$, the applied bias; $V_{bi}$, the built-in potential due to the difference in electrical contact work function; $V_a$, the voltage drop due to contact resistance and series resistance across the electrodes), and $L$ is the thickness of a photoactive layer. Current density versus voltage characteristics were recorded on a Keithley model 2400 source measuring unit.

Impedance measurements on encapsulated devices were conducted with a Solartron 1287 potentiostat and a Solartron 1260 frequency-response detector under 1 sun illumination at various applied potentials. The impedance response was measured over the range 1 Hz to 1 MHz with an oscillation amplitude of 10 mV. To extract the dielectric constant of blend films from a capacitance, the same measurements were also performed in the dark state.

Transient photovoltage (TPV) measurements were performed to determine charge carrier lifetime in OPV devices under 1 sun illumination at open circuit condition. Cells were pumped with a low-intensity nanosecond pulse at 520 nm (frequency of 1 Hz, pulse duration <1 ns), which introduced a small quantity ($\Delta V$ < 30 mV) of additional free carriers to the system.

## RESULTS AND DISCUSSION

Figure 1 shows the chemical structure of P3HT-Br10, a schematic representation of the photocrosslinking approach, and the device structures used in this study. P3HT-Br10 is a


dx.doi.org/10.1021/am404381e | ACS Appl. Mater. Interfaces 2014, 6, 333–339

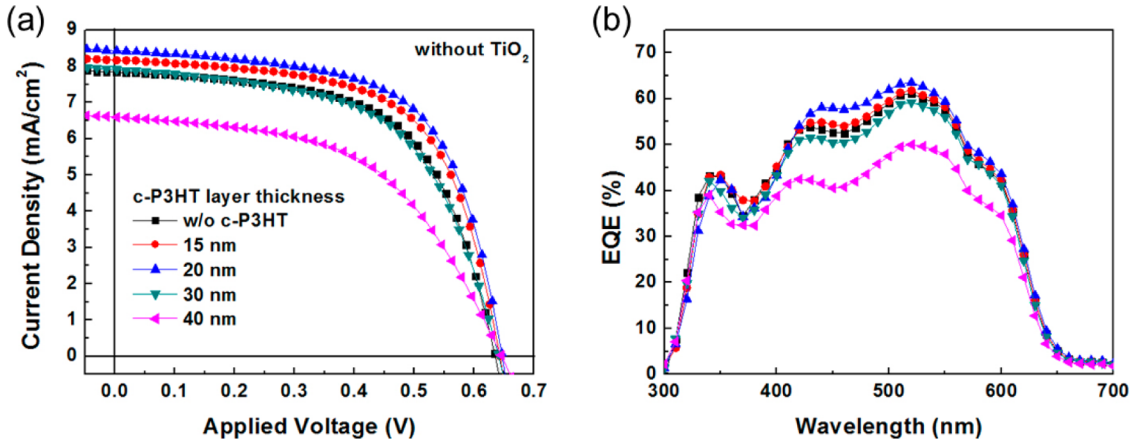


**Figure 2.** (a) Current density-voltage characteristics and (b) EQE spectra of ITO/PEDOT:PSS/c-P3HT/P3HT:PCBM/Al devices as a function of the thickness of the c-P3HT interlayer.

poly(3-hexylthiophene) copolymer containing 10% crosslinkable $\omega$-bromohexyl thiophene units (Figure 1a). The P3HT-Br10 polymers can be crosslinked via a radical mechanism initiated by the photochemical cleavage of the C−Br bonds under deep-UV irradiation at 254 nm,[38,41−44] as illustrated in Figure 1b. We confirmed that the thin c-P3HT layer was not soluble upon the spin-coating of P3HT:PCBM blend solution. The photocrosslinking behavior of the 20 nm thick P3HT-Br10 thin film was monitored using AFM (see the topographic images in Figure S1 (Supporting Information)). Prior to UV exposure, the P3HT-Br10 thin film was found to be very smooth, with an rms roughness ($R_q$) of 1.4 nm. After UV exposure for 1 min, a small portion of polymer chains became aggregated and was roughened to some degree ($R_q$ = 2.0 nm); however, the roughness of the c-P3HT film remained nearly identical to that of the PEDOT:PSS layer ($R_q$ = 2.0 nm). As a result, the P3HT:PCBM photoactive layer was formed either on the c-P3HT layer or on the PEDOT:PSS layer with nearly the same roughness values: $R_q$ = 0.79 and $R_q$ = 0.88 nm, respectively.

The effects of the c-P3HT layer on the device performance were examined by investigating the photovoltaic properties of P3HT:PCBM devices that incorporated different thickness values of the c-P3HT layers. Figure 2a shows the photocurrent density ($J$) versus voltage ($V$) curves obtained from ITO/PEDOT:PSS/c-P3HT/P3HT:PCBM/Al devices (Figure 1c) as a function of the c-P3HT film thickness (0−40 nm), measured under AM 1.5 G, 1 sun illumination. Table 1 summarizes the photovoltaic properties of the devices. Devices containing 15 and 20 nm thick c-P3HT interlayers showed improvements in the measured PCE values. Compared to the performances of the device prepared without a c-P3HT interlayer ($J_{SC}$ = 7.85 mA/cm$^2$), the best device containing a 20 nm thick c-P3HT layer yielded a $J_{SC}$ value of 8.42 mA/cm$^2$. The fill factor (FF) also increased slightly from 60.5 to 62.4%, resulting in a PCE improvement from 3.0 to 3.4%. By contrast, the devices prepared with 30 and 40 nm thick c-P3HT interlayers exhibited lower $J_{SC}$ and FF values. Figure 2b shows the external quantum efficiency (EQE) spectra of the devices. The devices prepared with 15−20 nm thick c-P3HT layers exhibited high EQEs throughout the visible range compared with devices prepared without the c-P3HT layer, in good agreement with the trend in $J_{SC}$ values shown in Figure 2a.

**Table 1. Photovoltaic Parameters of ITO/PEDOT:PSS/c-P3HT/P3HT:PCBM/Al Devices as a Function of the c-P3HT Thickness**

| thickness of c-P3HT | $V_{OC}$ (V) | $J_{SC}$ (mA/cm$^2$) | FF (%) | PCE (%) | $R_{series}$ (Ω) | $R_{shunt}$ (kΩ) |
|---|---|---|---|---|---|---|
| w/o c-P3HT | 0.64 | 7.85 | 60.5 | 3.0 | 120 | 11.1 |
| 15 nm | 0.64 | 8.16 | 62.0 | 3.2 | 104 | 11.9 |
| 20 nm | 0.65 | 8.42 | 62.4 | 3.4 | 101 | 10.4 |
| 30 nm | 0.64 | 7.91 | 57.8 | 2.9 | 152 | 8.2 |
| 40 nm | 0.65 | 6.59 | 52.7 | 2.3 | 228 | 7.7 |

This significant dependence of the c-P3HT thickness can be explained by changes in light absorption and series resistance accompanied by the incorporation of the c-P3HT layer. The c-P3HT layer may absorb some part of the UV−visible light before the P3HT:PCBM. Figure S2 (Supporting Information) shows the UV−visible absorption spectra of the various thick c-P3HT layers and the P3HT:PCBM layer. The light absorption of the 15 nm thick c-P3HT layer was negligible compared to that of the P3HT:PCBM layer. However, it is possible that the 20 nm thick c-P3HT film participates in generating extra excitons because of its nontrivial absorption, which would contribute to the increased $J_{SC}$ in some degree. The thicker c-P3HT films gave the lower $J_{SC}$ and FF values, because excitons formed in the thick c-P3HT films tend to recombine prior to encountering the PCBM molecules due to the exciton diffusion length of approximately 10−20 nm.[45,46] There is also a chance that the too thick c-P3HT films might reduce the light absorption in the P3HT:PCBM layer. Moreover, the series resistances of the device became appreciable in the very thick c-P3HT films due to the relatively low hole mobility of the c-P3HT layer, as observed in the measured $J$−$V$ characteristics (see Table 1).[23] For these reasons, the 20 nm thickness of the c-P3HT layer became optimal for its use as an electron blocking/hole extraction layer.

The more significant roles of the c-P3HT layer were thoroughly investigated with the 20 nm thick c-P3HT layer-incorporated devices by measuring hole mobilities and carrier lifetimes. The hole mobilities of the P3HT:PCBM and c-P3HT/P3HT:PCBM blend films were measured using the SCLC method. The incorporation of a 20 nm thick c-P3HT interlayer in the devices significantly increased the hole mobility from 1.03 × 10$^{-5}$ to 4.83 × 10$^{-5}$ cm$^2$ $V^{-1}$ s$^{-1}$. The higher hole mobility was attributed to the favorable hole extraction and


dx.doi.org/10.1021/am404381e | ACS Appl. Mater. Interfaces 2014, 6, 333−339

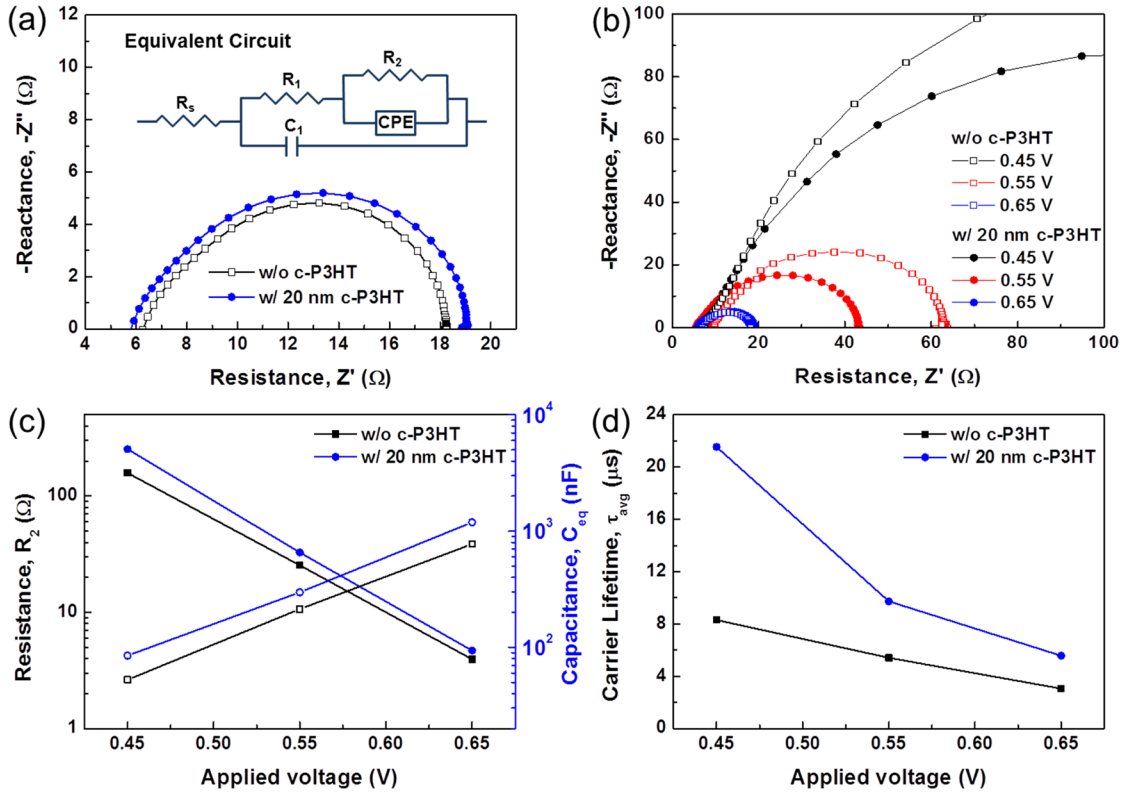


**Figure 3.** (a) Impedance response of P3HT:PCBM devices without and with the 20 nm thick c-P3HT interlayer at AM 1.5 G, 1 sun illumination at the open circuit conditions, (b) impedance response of P3HT:PCBM devices without and with the 20 nm thick c-P3HT interlayer at AM 1.5 G, 1 sun illumination at various applied voltages, (c) a semilog plot of recombination resistance and chemical capacitance versus applied voltage without and with the 20 nm thick c-P3HT interlayer, and (d) a plot of carrier lifetime $\tau_{avg}$ as a function of applied voltage without and with the 20 nm thick c-P3HT interlayer.

vertical composition distribution induced by the presence of the c-P3HT wetting layer between the P3HT:PCBM BHJ layer and the PEDOT:PSS film.[11] To confirm the vertical composition, we measured water contact angles of the P3HT:PCBM films on top of either the PEDOT:PSS layer or the c-P3HT layer and found that the P3HT:PCBM film on top of the c-P3HT layer showed a slightly lower contact angle of 76.6° than that of 81.1° without the c-P3HT layer (see Figure S3 in the Supporting Information). The lower contact angle from the P3HT:PCBM on top of the c-P3HT layer indicated that the top surface of the P3HT:PCBM was occupied more with the relatively more hydrophilic PCBM molecules, which is consistent with the favorable vertical composition.[22]

Impedance spectroscopy was performed to determine the key factors, such as the recombination resistance, chemical capacitance, and carrier lifetime, in a BHJ OPV device.[47,48] Figure 3a shows representative impedance responses of two partial semicircular arcs under open-circuit conditions. One might expect an additional semicircular arc when the c-P3HT layer was inserted because it is an extra layer and might generate a different interfacial contact between the PEDOT:PSS and the c-P3HT or between the c-P3HT and the P3HT:PCBM layer. However, no additional semicircular arc appeared upon the insertion of a c-P3HT interlayer in the device. Therefore, the same equivalent circuit model was applied for the devices without and with the c-P3HT interlayer in an effort to fit the impedance data of both devices. An equivalent circuit model employed by Leever et al.[49] was adopted (see the inset in Figure 3a). The $R_s$ circuit element represents the resistive losses through the entire device, including the contact resistance at the interfaces and the bulk resistance of the interfacial layers and the photoactive layer. This circuit element corresponds to the intersection of the semicircle on the Z′-axis at high frequencies.[49] The $R_s$ values were slightly lower for the device prepared with the c-P3HT layer ($R_s$ = 6.21 Ω) than for the device prepared without a c-P3HT layer ($R_s$ = 6.69 Ω), presumably because the series resistance was reduced or the hole mobility in the c-P3HT/P3HT:PCBM blend was increased. The high frequency arc is represented by an $R_1\|C_1$ combination and is related to the bulk resistance and capacitance. This arc includes a geometric component and another component related to photocarrier generation. The larger arc in the low frequency region is characterized by an $R_2\|$CPE combination, where $R_2$ accounts for the recombination resistance, and the constant phase element (CPE) includes a component of the chemical capacitance ($C_{eq}$) at the charge transfer event between donors and acceptors in the photoactive blend.[50,51] Impedance responses at low voltages were also obtained (Figure 3b). The impedance data of the devices were fit to determine $R_2$ and $C_{eq}$. We then calculated the average carrier lifetime constant ($\tau_{avg}$) using the following equation:

$$\tau_{avg} = R_2 C_{eq} \quad (3)$$

Figure 3c,d presents the extracted $R_2$, $C_{eq}$, and $\tau_{avg}$ values as a function of the applied voltage under AM 1.5 G, 1 sun illumination. These results and data range agreed well with previous reports.[49,52] As the applied voltage was increased, $R_2$ decreased exponentially whereas $C_{eq}$ increased exponentially. These trends resulted from the exponential increase in charge

carrier injection into the photoactive layer as the applied voltage was increased.[49,52] Importantly, the average $\tau_{avg}$ values of the devices prepared with a c-P3HT interlayer were much larger than the values obtained from the corresponding devices prepared without a c-P3HT interlayer, especially at lower applied voltages. For instance, at 0.45 V, $\tau_{avg}$ in the device prepared with a c-P3HT layer ($\tau_{avg}$ = 22 $\mu$s) was approximately three times larger than $\tau_{avg}$ in the device prepared without a c-P3HT layer ($\tau_{avg}$ = 8 $\mu$s). As the voltage increased, the $\tau_{avg}$ values of the devices prepared without or with the c-P3HT layer decreased gradually, and the difference between the values decreased. At an applied voltage of 0.65 V, $\tau_{avg}$ in the device prepared with a c-P3HT layer ($\tau_{avg}$ = 6 $\mu$s) remained twice the value obtained from a device prepared without a c-P3HT layer ($\tau_{avg}$ = 3 $\mu$s). These results indicated that the recombination rate in the device prepared with a c-P3HT interlayer decreased significantly.

TPV measurements were conducted under AM 1.5 G, 1 sun illumination under open-circuit conditions. The TPV technique was used to interrogate the microsecond processes that occurred in photovoltaic devices, as reported previously.[53] Figure 4 displays representative TPV signals obtained from devices prepared without or with a c-P3HT layer, respectively. The TPV signals produced at a cell by the presence of excess carriers upon transient light exposure, showed a monoexponential decay. The carrier lifetimes were extracted from the device by fitting the transient photovoltage profile using the following equation:

$$\Delta V \propto \exp(-t/\tau) \quad (4)$$

where $\Delta V$ is the photovoltage change upon irradiation of a nanosecond pulse of a 520 nm laser beam with respect to the $V_{OC}$, $t$ is time, and $\tau$ is the carrier lifetime. The carrier lifetimes of the OPV devices prepared without or with the c-P3HT interlayer were determined to be 6 or 27 $\mu$s, respectively. The trend in the TPV data was consistent with the results obtained from the impedance spectra, and the values were within an acceptable range, according to the previous reports.[53,54] The agreement with previous results demonstrated that the charge carrier lifetimes of the OPV devices could be enhanced by inserting a hole-blocking interlayer.[32,53]

The device performance was further enhanced by incorporating an additional $TiO_2$ nanoparticle layer to produce the device structure: ITO/PEDOT:PSS/c-P3HT/P3HT:PCBM/$TiO_2$/Al (Figure 1 d). The solution-processed $TiO_2$ nanoparticle layer can bring a positive contribution to the device performance by acting as an optical spacer and as a hole blocker.[32,55,56] The $TiO_2$ layer suppressed the leakage current and recombination near the active/Al interface.[32] Figure 5a shows the photocurrent density ($J$) versus voltage ($V$) curves obtained from the devices as a function of the c-P3HT thickness, measured under AM 1.5 G, 1 sun illumination. Table 2 summarizes the photovoltaic parameters of the devices prepared with a $TiO_2$ nanoparticle layer. The insertion of the $TiO_2$ nanoparticle layer improved the PCE from 3.0 to 3.6%. The additional introduction of a c-P3HT layer further increased the PCE of the device prepared with a 15 or 20 nm thick c-

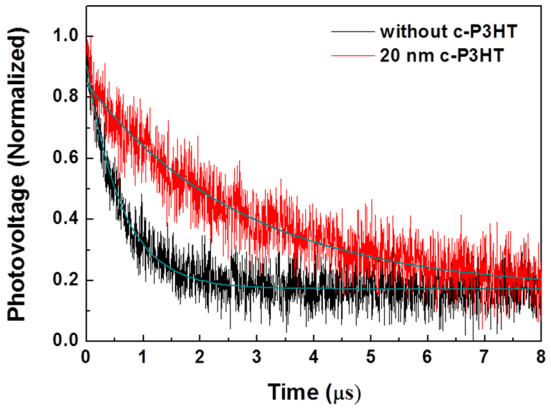


**Figure 4.** TPV response profiles of the ITO/PEDOT:PSS/P3HT:PCBM/Al devices without and with the 20 nm thick c-P3HT interlayer under AM 1.5 G, 1 sun illumination.

**Table 2. Photovoltaic Parameters of ITO/PEDOT:PSS/c-P3HT/P3HT:PCBM/$TiO_2$/Al Devices as a Function of the c-P3HT Thickness**

| thickness of c-P3HT | $V_{OC}$ (V) | $J_{SC}$ (mA/cm$^2$) | FF (%) | PCE (%) | $R_{series}$ (Ω) | $R_{shunt}$ (kΩ) |
|---|---|---|---|---|---|---|
| w/o c-P3HT | 0.66 | 8.08 | 68.2 | 3.6 | 79.8 | 12.2 |
| 15 nm | 0.65 | 8.49 | 69.4 | 3.8 | 68.5 | 14.2 |
| 20 nm | 0.66 | 8.74 | 70.1 | 4.0 | 64.8 | 12.2 |
| 30 nm | 0.67 | 7.92 | 65.0 | 3.4 | 85.8 | 12.0 |
| 40 nm | 0.66 | 7.05 | 57.6 | 2.7 | 102 | 9.1 |

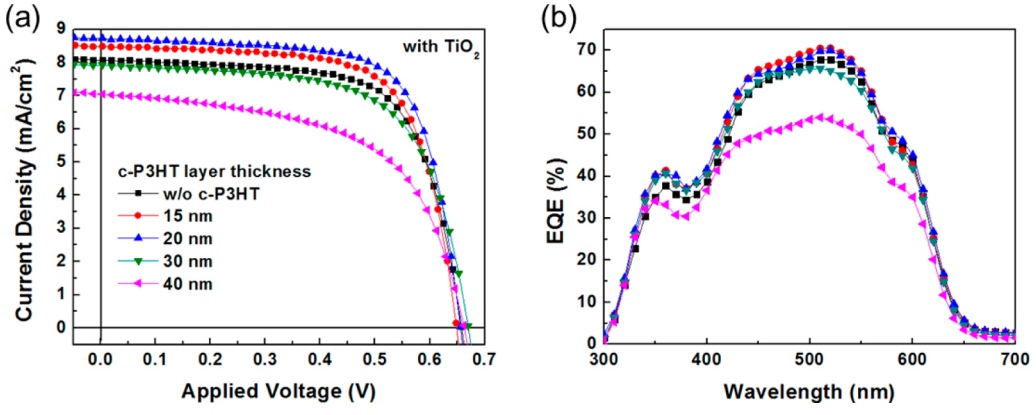


**Figure 5.** (a) Current density-voltage characteristics and (b) EQE spectra of ITO/PEDOT:PSS/c-P3HT/P3HT:PCBM/$TiO_2$/Al devices as a function of the thickness of the c-P3HT interlayer.

P3HT layer, whereas the devices prepared with 30 or 40 nm thick c-P3HT layers exhibited lower $J_{SC}$ and FF values. This trend was the same as that observed in devices prepared without a $TiO_2$ nanoparticle layer. The optimal thickness of the c-P3HT layer was found to be 20 nm again, and the PCE increased significantly to 4.0%. A notable increase in the $J_{SC}$ and FF values was observed, from 8.08 mA/cm$^2$ and 68.2% for the device prepared without a c-P3HT layer to 8.74 mA/cm$^2$ and 70.1% for the device prepared with a 20 nm thick c-P3HT layer. Note that the incorporation of both the c-P3HT and the $TiO_2$ layers resulted in a significant synergetic effect on the PCEs, which increased from 3.0% (the PCE without both the layers) to 4.0% (the PCE with both the layers). Figure 5b displays the EQE spectra of the devices. It should be emphasized that the EQE values improved over the entire wavelength range 300–650 nm, and the EQE max values increased considerably, from 61% for the basic structured device to 70.5%. This observation suggested that the $TiO_2$ layer significantly suppressed the carrier recombination at the photoactive layer/Al interfaces while the c-P3HT layer prevented carrier recombination at the interface between the PEDOT:PSS and P3HT:PCBM blend layers.

The reduced recombination and improved PCE values, obtained through the use of the c-P3HT and $TiO_2$ layers, could be explained in terms of the schematic energy level diagram for the ITO/PEDOT:PSS/c-P3HT/P3HT:PCBM/$TiO_2$/Al structure (Figure 6). The levels of the highest occupied molecular orbital (HOMO) and lowest unoccupied molecular orbital (LUMO) in c-P3HT were expected to be the same as the corresponding levels of the P3HT polymer in a P3HT:PCBM blend layer, which can create a homogeneous pathway towards the PEDOT:PSS layer for hole transport. The electrons could be blocked by the c-P3HT layer because the LUMO level of the c-P3HT was higher than that of the PCBM layer. The $TiO_2$ layer formed a nearly ohmic contact with the Al electrode, allowing for efficient electron collection while effectively blocking holes. In this manner, nongeminate recombination at the photoactive/electrode interfaces could be significantly reduced, as strongly supported by the carrier lifetime measurement data.

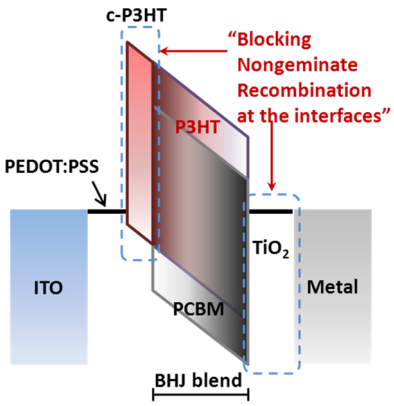


**Figure 6.** Schematic energy diagram of the OPV device with ITO/PEDOT:PSS/c-P3HT/P3HT:PCBM/$TiO_2$/Al structures, where the c-P3HT and $TiO_2$ layers prevent nongeminate recombination at the interfaces.

## CONCLUSIONS

We described the important role of a c-P3HT electron blocking/hole extraction layer in a device prepared with the structure ITO/PEDOT:PSS/c-P3HT/P3HT:PCBM/Al. The insertion of the c-P3HT layer considerably improved the device performance. The hole mobility and carrier lifetime measurements revealed that the c-P3HT interlayer facilitated hole transport and lengthened the carrier lifetime by preventing nongeminate recombination at the interface between the PEDOT:PSS and the P3HT:PCBM photoactive layer. We found that the $TiO_2$ hole blocking/electron extraction layer synergistically promoted the photovoltaic properties when incorporated into a device having a c-P3HT layer by preventing additional nongeminate recombination at the interface between the photoactive layer and the Al electrode. This work demonstrates that the placement of a robust photocrosslinkable polymer layer and a metal oxide layer between the photoactive layer and electrodes is critical for extending the carrier lifetime and improving effective carrier transport/extraction. This strategy is expected to be applicable to other polymer-based photovoltaic systems to enhance the performances of those systems.

## ASSOCIATED CONTENT

### Supporting Information

AFM images of polymer and photoactive films (Figure S1), UV–visible absorption spectra of the various thick c-P3HT layers (Figure S2), and water contact angles of the P3HT:PCBM layers (Figure S3). This material is available free of charge via the Internet at http://pubs.acs.org.

## AUTHOR INFORMATION

### Corresponding Author

*B.-S. Kim. E-mail: bongsoo@kist.re.kr.

### Notes

The authors declare no competing financial interest.

## ACKNOWLEDGMENTS

This work was supported by New and Renewable Energy Program of the Korea Institute of Energy Technology Evaluation and Planning (KETEP) grant funded by the Ministry of Trade, Industry & Energy (MTIE) (20113030010060) and by Korea Research Council of Fundamental Science and Technology (KRCF) and Korea Institute of Science and Technology (KIST) for "NAP National Agenda Project Program" and Project No. 2E23821, and by the National Research Foundation of Korea Grant funded by the Korean Government (MSIP) (2013, University-Institute corporation program).

## REFERENCES

(1) Krebs, F. C.; Gevorgyan, S. A.; Alstrup, J. *J. Mater. Chem.* **2009**, *19*, 5442–5451.
(2) Shaheen, S. E.; Radspinner, R.; Peyghambarian, N.; Jabbour, G. E. *Appl. Phys. Lett.* **2001**, *79*, 2996–2998.
(3) Steirer, K. X.; Berry, J. J.; Reese, M. O.; van Hest, M. F. A. M.; Miedaner, A.; Liberatore, M. W.; Collins, R. T.; Ginley, D. S. *Thin Solid Films* **2009**, *517*, 2781–2786.
(4) Thompson, B. C.; Frechet, J. M. J. *Angew. Chem., Int. Ed.* **2008**, *47*, 58–77.
(5) Guo, F.; Zhu, X.; Forberich, K.; Krantz, J.; Stubhan, T.; Salinas, M.; Halik, M.; Spallek, S.; Butz, B.; Spiecker, E.; et al. *Adv. Energy Mater.* **2013**, *3*, 1062–1067.

(6) Kymakis, E.; Savva, K.; Stylianakis, M. M.; Fotakis, C.; Stratakis, E. *Adv. Funct. Mater.* **2013**, *23*, 2742−2749.
(7) Liang, Y. Y.; Xu, Z.; Xia, J. B.; Tsai, S. T.; Wu, Y.; Li, G.; Ray, C.; Yu, L. P. *Adv. Mater.* **2010**, *22*, E135−E138.
(8) Service, R. F. *Science* **2011**, *332*, 293−293.
(9) Son, H. J.; Lu, L. Y.; Chen, W.; Xu, T.; Zheng, T. Y.; Carsten, B.; Strzalka, J.; Darling, S. B.; Chen, L. X.; Yu, L. P. *Adv. Mater.* **2013**, *25*, 838−843.
(10) Hendriks, K. H.; Heintges, G. H. L.; Gevaerts, V. S.; Wienk, M. M.; Janssen, R. A. J. *Angew. Chem., Int. Ed.* **2013**, *52*, 8341−8344.
(11) Cabanetos, C.; El Labban, A.; Bartelt, J. A.; Douglas, J. D.; Mateker, W. R.; Fréchet, J. M. J.; McGehee, M. D.; Beaujuge, P. M. *J. Am. Chem. Soc.* **2013**, *135*, 4656−4659.
(12) Wu, Y.; Li, Z.; Ma, W.; Huang, Y.; Huo, L.; Guo, X.; Zhang, M.; Ade, H.; Hou, J. *Adv. Mater.* **2013**, *25*, 3449−3455.
(13) Sariciftci, N. S.; Smilowitz, L.; Heeger, A. J.; Wudl, F. *Science* **1992**, *258*, 1474−1476.
(14) Yu, G.; Gao, J.; Hummelen, J. C.; Wudl, F.; Heeger, A. J. *Science* **1995**, *270*, 1789−1791.
(15) Choi, H.; Kim, B.; Ko, M. J.; Lee, D. K.; Kim, H.; Kim, S. H.; Kim, K. *Org. Electron.* **2012**, *13*, 959−968.
(16) Li, G.; Shrotriya, V.; Huang, J. S.; Yao, Y.; Moriarty, T.; Emery, K.; Yang, Y. *Nat. Mater.* **2005**, *4*, 864−868.
(17) Ma, W. L.; Yang, C. Y.; Gong, X.; Lee, K.; Heeger, A. J. *Adv. Funct. Mater.* **2005**, *15*, 1617−1622.
(18) Bjorstrom, C. M.; Bernasik, A.; Rysz, J.; Budkowski, A.; Nilsson, S.; Svensson, M.; Andersson, M. R.; Magnusson, K. O.; Moons, E. *J. Phys-Condens. Mat.* **2005**, *17*, L529−L534.
(19) Campoy-Quiles, M.; Ferenczi, T.; Agostinelli, T.; Etchegoin, P. G.; Kim, Y.; Anthopoulos, T. D.; Stavrinou, P. N.; Bradley, D. D. C.; Nelson, J. *Nat. Mater.* **2008**, *7*, 158−164.
(20) Xu, Z.; Chen, L. M.; Yang, G. W.; Huang, C. H.; Hou, J. H.; Wu, Y.; Li, G.; Hsu, C. S.; Yang, Y. *Adv. Funct. Mater.* **2009**, *19*, 1227−1234.
(21) Yao, Y.; Hou, J. H.; Xu, Z.; Li, G.; Yang, Y. *Adv. Funct. Mater.* **2008**, *18*, 1783−1789.
(22) Oh, J. Y.; Jang, W. S.; Lee, T. I.; Myoung, J. M.; Baik, H. K. *Appl. Phys. Lett.* **2011**, *98*, 023303.
(23) Zhang, Y.; Dang, X. D.; Kim, C.; Nguyen, T. Q. *Adv. Energy Mater.* **2011**, *1*, 610−617.
(24) Credgington, D.; Jamieson, F. C.; Walker, B.; Nguyen, T. Q.; Durrant, J. R. *Adv. Mater.* **2012**, *24*, 2135−2141.
(25) Kumar, A.; Li, G.; Hong, Z. R.; Yang, Y. *Nanotechnology* **2009**, *20*, 165202.
(26) Wei, Q. S.; Nishizawa, T.; Tajima, K.; Hashimoto, K. *Adv. Mater.* **2008**, *20*, 2211−2216.
(27) Chen, Y.; Jiang, Z. T.; Gao, M.; Watkins, S. E.; Lu, P.; Wang, H. Q.; Chen, X. W. *Appl. Phys. Lett.* **2012**, *100*, 203304.
(28) Irwin, M. D.; Servaites, J. D.; Buchholz, D. B.; Leever, B. J.; Liu, J.; Emery, J. D.; Zhang, M.; Song, J. H.; Durstock, M. F.; Freeman, A. J.; et al. *Chem. Mater.* **2011**, *23*, 2218−2226.
(29) Jasieniak, J. J.; Seifter, J.; Jo, J.; Mates, T.; Heeger, A. J. *Adv. Funct. Mater.* **2012**, *22*, 2594−2605.
(30) Yoon, S. J.; Park, J. H.; Lee, H. K.; Park, O. O. *Appl. Phys. Lett.* **2008**, *92*, 143504.
(31) Cheng, Y. J.; Hsieh, C. H.; He, Y. J.; Hsu, C. S.; Li, Y. F. *J. Am. Chem. Soc.* **2010**, *132*, 17381−17383.
(32) Kim, Y. S.; Kim, T.; Kim, B.; Lee, D. K.; Kim, H.; Ju, B. K.; Kim, K. *Org. Electron.* **2013**, *14*, 1749−1754.
(33) You, J.; Dou, L.; Yoshimura, K.; Kato, T.; Ohya, K.; Moriarty, T.; Emery, K.; Chen, C.-C.; Gao, J.; Li, G.; et al. *Nat. Commun.* **2013**, *4*, 1446.
(34) Kyaw, A. K. K.; Wang, D. H.; Wynands, D.; Zhang, J.; Nguyen, T.-Q.; Bazan, G. C.; Heeger, A. J. *Nano Lett.* **2013**, *13*, 3796−3801.
(35) Mbule, P. S.; Kim, T. H.; Kim, B. S.; Swart, H. C.; Ntwaeaborwa, O. M. *Sol. Energy Mater. Sol. Cells* **2013**, *112*, 6−12.
(36) Stratakis, E.; Stylianakis, M. M.; Koudoumas, E.; Kymakis, E. *Nanoscale* **2013**, *5*, 4144−4150.
(37) Tong, S. W.; Zhang, C. F.; Jiang, C. Y.; Liu, G.; Ling, Q. D.; Kang, E. T.; Chan, D. S. H.; Zhu, C. X. *Chem. Phys. Lett.* **2008**, *453*, 73−76.
(38) Kim, B. J.; Miyamoto, Y.; Ma, B. W.; Fréchet, J. M. J. *Adv. Funct. Mater.* **2009**, *19*, 2273−2281.
(39) Kim, H. J.; Han, A. R.; Cho, C.-H.; Kang, H.; Cho, H.-H.; Lee, M. Y.; Fréchet, J. M. J.; Oh, J. H.; Kim, B. J. *Chem. Mater.* **2011**, *24*, 215−221.
(40) Chung, W. S.; Lee, H.; Lee, W.; Ko, M. J.; Park, N. G.; Ju, B. K.; Kim, K. *Org. Electron.* **2010**, *11*, 521−528.
(41) Woo, C. H.; Piliego, C.; Holcombe, T. W.; Toney, M. F.; Fréchet, J. M. J. *Macromolecules* **2012**, *45*, 3057−3062.
(42) Lee, K. S.; Yeon, K. Y.; Jung, K. H.; Kim, S. K. *J. Phys. Chem. A* **2008**, *112*, 9312−9317.
(43) Lee, Y. R.; Chen, C. C.; Lin, S. M. *J. Chem. Phys.* **2003**, *118*, 10494−10501.
(44) Tang, Y.; Ji, L.; Zhu, R. S.; Wei, Z. R.; Zhang, B. *J. Phys. Chem. A* **2005**, *109*, 11123−11126.
(45) Shaw, P. E.; Ruseckas, A.; Samuel, I. D. W. *Adv. Mater.* **2008**, *20*, 3516−3520.
(46) Markov, D. E.; Amsterdam, E.; Blom, P. W. M.; Sieval, A. B.; Hummelen, J. C. *J. Phys. Chem. A* **2005**, *109*, 5266−5274.
(47) Garcia-Belmonte, G.; Boix, P. P.; Bisquert, J.; Lenes, M.; Bolink, H. J.; La Rosa, A.; Filippone, S.; Martin, N. *J. Phys. Chem. Lett.* **2010**, *1*, 2566−2571.
(48) Garcia-Belmonte, G.; Boix, P. P.; Bisquert, J.; Sessolo, M.; Bolink, H. J. *Sol. Energy Mater. Sol. Cells* **2010**, *94*, 366−375.
(49) Leever, B. J.; Bailey, C. A.; Marks, T. J.; Hersam, M. C.; Durstock, M. F. *Adv. Energy Mater.* **2012**, *2*, 120−128.
(50) Jovanovski, V.; Gonzalez-Pedro, V.; Gimenez, S.; Azaceta, E.; Cabanero, G.; Grande, H.; Tena-Zaera, R.; Mora-Sero, I.; Bisquert, J. *J. Am. Chem. Soc.* **2011**, *133*, 20156−20159.
(51) Leong, W. L.; Cowan, S. R.; Heeger, A. J. *Adv. Energy Mater.* **2011**, *1*, 517−522.
(52) Fabregat-Santiago, F.; Garcia-Belmonte, G.; Mora-Sero, I.; Bisquert, J. *Phys. Chem. Chem. Phys.* **2011**, *13*, 9083−9118.
(53) Shuttle, C. G.; O'Regan, B.; Ballantyne, A. M.; Nelson, J.; Bradley, D. D. C.; de Mello, J.; Durrant, J. R. *Appl. Phys. Lett.* **2008**, *92*, 093311.
(54) Boix, P. P.; Ajuria, J.; Pacios, R.; Garcia-Belmonte, G. *J. Appl. Phys.* **2011**, *109*, 074514.
(55) Roy, A.; Park, S. H.; Cowan, S.; Tong, M. H.; Cho, S.; Lee, K.; Heeger, A. J. *Appl. Phys. Lett.* **2009**, *95*, 013302.
(56) Kim, J. Y.; Kim, S. H.; Lee, H. H.; Lee, K.; Ma, W.; Gong, X.; Heeger, A. J. *Adv. Mater.* **2006**, *18*, 572−576.